Impacts of Heterogeneous Chemistry on Vertical Profiles of Martian Ozone

M. A. J. Brown[1], M. R. Patel[1,2], S. R. Lewis[1], J. A. Holmes[1], G. J. Sellers[1], P. M. Streeter[1], A. Bennaceur[1], G. Liuzzi[3,4], G. L. Villanueva[3], A. C. Vandaele[5]

[1]The Open University, Milton Keynes, U.K.
[2]Space Science and Technology Department, Science and Technology Facilities Council, Rutherford Appleton Laboratory, Oxfordshire, U.K.
[3]Planetary Systems Laboratory, NASA Goddard Space Flight Center, Greenbelt, MD, USA
[4]Department of Physics, American University, Washington, DC, USA
[5]Royal Belgian Institute for Space Aeronomy (BIRA-IASB), Brussels, Belgium

Key Points:

- Ozone and water ice profiles show a positive vertical correlation, contrary to global ozone and water vapour total column anti-correlation
- Heterogeneous chemistry increases ozone abundance at altitudes where water ice is present, matching locations where ozone is underpredicted
- High hydroxyl radical abundance, assumed proportional to high water vapour abundance, masks the effects of heterogeneous chemistry on ozone

Corresponding author: M.A.J. Brown, `megan.brown@open.ac.uk`

Abstract

We show a positive vertical correlation between ozone and water ice using a vertical cross-correlation analysis with observations from the ExoMars Trace Gas Orbiter's NOMAD instrument. We find this is particularly apparent during the first half of Mars Year 35 ($L_S = 0° - 180°$) at high southern latitudes, when the water vapour abundance is low. This contradicts the current understanding that ozone and water are, in general, anti-correlated. However, our simulations with gas-phase-only chemistry using a 1-D model show that ozone concentration is not influenced by water ice. Heterogeneous chemistry has been proposed as a mechanism to explain the underprediction of ozone in global climate models (GCMs) through the removal of HO_x. We find improving the heterogeneous chemical scheme causes ozone abundance to increase when water ice is present, better matching observed trends. When water vapour abundance is high, there is no consistent vertical correlation between observed ozone and water ice and, in simulated scenarios, the heterogeneous chemistry does not have a large influence on ozone. HO_x, which are by-products of water vapour, dominate ozone abundance and mask the effects of heterogeneous chemistry on ozone. This is consistent with gas-phase-only modelled ozone, showing good agreement with observations when water vapour is abundant. High water vapour abundance masks the effect of heterogeneous reactions on ozone abundance and makes adsorption of HO_x have a negligible impact on ozone. Overall, the inclusion of heterogeneous chemistry improves the ozone vertical structure in regions of low water vapour abundance, which may partially explain GCM ozone deficits.

Plain Language Summary

Ozone gas is found in small quantities in the martian atmosphere, highly variable both in time and space. Ozone quantity is controlled by photochemical reactions involving other species too difficult to detect with remote sensing. Two main ways ozone is destroyed in the martian atmosphere are by: 1. absorbing ultraviolet sunlight; 2. reacting with hydroxyl radicals, highly reactive chemical formed by water vapour absorbing ultraviolet sunlight. The latter leads to a well-known anti-correlation between ozone and water vapour. Ozone is underpredicted in climate models, implying chemical reactions are missing or incorrect in models. We investigate reactions between hydroxyl radicals and water ice as a potential explanation for the ozone underprediction by using a model and observed vertical profiles. We find observed ozone and water ice have a positive vertical correlation and, when simulating a model with improved chemistry, ozone abundance increases at altitudes where water ice is present due to the decrease in hydroxyl radicals. However, in areas where water vapour is abundant, no such correlation is seen and the chemistry has little impact on modelled ozone. This is due to large abundances of hydroxyl radicals which inhibit the increase in ozone caused by the addition of the improved chemistry.

1 Introduction

1.1 Background

Ozone on Mars was first detected in 1969 by Mariner 7 and later by Mariner 9. It was found to vary seasonally in both hemispheres, with a greater abundance in local winter which decreased during the local summer (Barth et al., 1973). Other instruments, such as SPICAM (Spectroscopy for the Investigation of the Characteristics of the Atmosphere of Mars) aboard Mars Express (Bertaux et al., 2006), MARCI (Mars Colour Imager) aboard Mars Reconnaissance Orbiter (Bell III et al., 2009), and NOMAD (Nadir and Occultation for Mars Discovery) aboard the ExoMars Trace Gas Orbiter (TGO) (M. R. Patel et al., 2017; Vandaele et al., 2018) later confirmed the seasonal variability, and ob-

servations show that the highest abundance of ozone occurs at high latitudes (e.g. Perrier et al. (2006); Clancy et al. (2016); M. R. Patel et al. (2021); Khayat et al. (2021)).

In the martian atmosphere, ozone is a trace gas highly sensitive to direct (photolysis) and indirect (reactions with photolysised products) photochemical reactions. Due to its sensitivity to other chemical species and its relatively short lifetime (2-3 hours on the dayside), ozone is often a useful indicator of the chemical reactions occurring in the atmosphere (Clancy & Nair, 1996). One of the main destructive pathways of ozone is via reactions with hydroxyl radicals (OH, HO_2; HO_x) and atomic hydrogen, H, which are a by-product of the photolysis of water vapour (Shimazaki & Shimizu, 1979; Clancy & Nair, 1996; Lefèvre et al., 2004). HO_x are highly reactive and cause a set of chain reactions which produce more HO_x and lead to further ozone destruction. Their high reactivity makes them a key component in understanding the stability of the martian atmosphere as they catalyse the recombination of atomic oxygen and carbon monoxide to form carbon dioxide (McElroy & Donahue, 1972; Clancy & Nair, 1996). The destructive pathway of ozone caused by HO_x results in a photochemical anti-correlation between ozone and water vapour. As a result, the seasonal variation in ozone is influenced by the fluctuation in water vapour throughout the year.

The seasonal cycle and asymmetric distribution of water vapour between the two hemispheres leads to a larger ozone abundance at high southern latitudes during southern winter, compared to high northern latitudes during northern winter (Perrier et al., 2006; Montmessin & Lefèvre, 2013). So far, the highest recorded abundances of ozone have occurred at high southern latitudes ($> 55°$ S) between the northern spring equinox and the northern autumnal equinox ($L_S = 0°-180°$). Global climate models (GCMs) are also in agreement with these findings (Lefèvre et al., 2004; Perrier et al., 2006; Clancy et al., 2016; J. A. Holmes et al., 2018).

Similarly, water ice has been detected at high latitudes between $L_S = 0° - 180°$ (e.g. Smith (2004); Benson et al. (2010, 2011); Wolff et al. (2019)). During the northern and southern winters, water vapour condenses over the polar regions and forms water-ice clouds known as the North and South Polar Hood respectively (Benson et al., 2010, 2011). The North Polar Hood lasts from $L_S = 150°$ to $L_S = 30°$ the following year, while the South Polar Hood is observed between $L_S = 10° - 200°$. Clancy et al. (2016) and Daerden et al. (2019) showed that the greatest underprediction of ozone occurs between $L_S = 0° - 180°$ at high ($> 60°$ N/S) latitudes, as compared against MARCI observations. Lefèvre et al. (2008) found that ozone was underpredicted throughout the year across all latitudes, although the largest differences between the modelled and observed data from SPICAM were also between $L_S = 0° - 180°$ at high northern and southern latitudes. M. R. Patel et al. (2021) showed that the greatest underprediction of ozone occurs in the southern hemisphere at low altitudes in the vertical profile also between $L_S = 0° - 180°$.

Due to the chemical sensitivity of ozone, an ozone deficit can be used as a proxy for missing or undeveloped chemical reactions in atmospheric models (Nair et al., 1994; Lefèvre et al., 2008). Anbar et al. (1993) suggested ozone abundance could be increased by adding heterogeneous chemistry, in the form of incorporating the adsorption of HO_x onto the surface of water ice. They used a 1-dimensional (1-D) model to simulate this chemistry, and found that the water ice acted as a sink for HO_x, reducing the destruction rate of ozone and resulting in an enhanced ozone abundance. Lefèvre et al. (2004) briefly mentioned that heterogeneous chemistry could increase the ozone abundance as it was still underpredicted in a 3-D model. This was further developed by Lefèvre et al. (2008) who included 2 heterogeneous reactions with OH and HO_2 in their model and found that the addition of these reactions increased the total ozone column abundance; the results were in better agreement with SPICAM total ozone column measurements than the gas-only simulation, although ozone in their 3-D model was overpredicted at low latitudes during the aphelion season (between $L_S = 60° - 150°$). However, Clancy et al.

(2016) found that the simulated ozone with the heterogeneous chemistry was not in agreement with MARCI total ozone column and, using the relationship between ozone and water ice as a proxy for heterogeneous reactions, found that the observed and simulated data had different correlations between ozone and water ice. They concluded that the observations did not show sufficient evidence of heterogeneous processes.

Lefèvre et al. (2021) used an adaptive semi-implicit scheme (ASIS) taken from Cariolle et al. (2017) to improve the chemical timestep and stability of the GCM. In constrast to previous studies, which had overestimated the water ice optical depth, this study had improved the water ice optical depth to be in better agreement with observations. These changes improved the agreement between simulated total ozone column and observed total ozone column from SPICAM at high northern latitudes. They found that the inclusion of heterogeneous chemistry enhanced ozone abundance at high northern latitudes and was in strong agreement with SPICAM observations. The simulated water vapour was also in good agreement with total water vapour columns from SPICAM observations, although water vapour was overpredicted in some regions (e.g. low latitudes in aphelion, southern latitudes during southern summer). Water vapour is a key species to investigating the effect of heterogeneous chemistry since it is directly related to the abundance of HO_x. For Lefèvre et al. (2021), ozone abundance was still underpredicted in some scenarios when water vapour abundance was low, but matched when water vapour abundance was higher ($> 1\,\mathrm{pr}$-μm).

The adsorption of HO_x onto water ice is a physical process rather than chemical, and thus the method for modelling heterogeneous reactions is ambiguous as there are no definitive chemical reactions. Lefèvre et al. (2008) did not define any products for the heterogeneous reactions, and Lefèvre et al. (2021) later included oxygen and water vapour as products to conserve mass. Modelling of ozone has shown mixed results in explaining observed data and there are still many outstanding problems (Lefèvre et al., 2008; Clancy et al., 2016; Lefèvre et al., 2021). All studies regarding heterogeneous chemistry have used ozone total column abundance in their investigations, which has a major drawback of only revealing the net difference in ozone throughout the column. In contrast, vertical profiles show the full vertical distribution of species (e.g. ozone and water ice) and, since the species can be viewed as mixing ratios rather than abundances, the relationship between ozone and water ice can be studied with equal weighting across all altitudes. Confirming the presence of ozone and water ice at the same altitudes is crucial to investigating the relationship between the two species as, without defining the vertical distribution, it is difficult to verify any impact heterogeneous reactions have on ozone. Determining the chemical impacts of heterogeneous reactions on both the total abundance and vertical distribution of ozone is essential to understanding how ozone is expected to vary indirectly under the influence of heterogeneous reactions.

1.2 Outline

This study uses a combination of statistical analysis and 1-dimensional (1-D) modelling to quantify the impacts of heterogeneous reactions on ozone vertical profiles under different circumstances. We analyse observed vertical profiles of ozone and water ice at high ($> 45°$) northern and southern latitudes between $L_S = 0° - 180°$ using a vertical cross-correlation analysis to determine the relationship between observed ozone and water ice. We then use a 1-D model with an improved heterogeneous chemical scheme to compare vertical profiles of simulated ozone with and without the heterogeneous chemistry to determine the impact of heterogeneous reactions. We compare a high and a low water vapour abundance scenario to replicate the atmospheric state in the northern summer and southern winter respectively, and assess the influence of heterogeneous chemistry on ozone under such conditions.

Section 2 describes the vertical profiles from NOMAD, the vertical cross-correlation analysis, and the improved chemical scheme used in the 1-D model. Section 3 describes the results of the cross-correlation analysis between ozone and water ice, and the ozone variation in the 1-D model in low and high water vapour abundance scenarios. Finally, Section 4 discusses the impact of water ice on ozone, and the influence of water vapour on heterogeneous chemistry, before summarising the conclusions and implications of the study.

2 Methods

2.1 NOMAD Profiles

Ozone and water ice vertical profiles used in this study are derived respectively from the UVIS (UV-Visible) spectrometer and the SO (Solar Occultation) spectrometer on the NOMAD instrument aboard TGO, detailed in M. R. Patel et al. (2021) and Liuzzi et al. (2020). Data cover high latitudes ($> 45°$ N/S) from $L_S = 0°-180°$ MY 35 and, as there is little zonal variation, all longitudes are included together. Data between $L_S = 0°-30°$ are omitted for the high northern latitudes analysis due to an absence of data below $30\,km$ in ozone and water vapour profiles. Between $L_S\ 30°-180°$ at the high northern latitudes, there is a much lower ozone abundance (up to $0.1\,ppmv$) and thus there are fewer ozone profiles which meet the minimum requirement for the analysis (Table 1). This still leaves 300 profile pairs which meet the conditions set for the cross-correlation.

Solar occultations profile the atmosphere at the terminator and can occur up to 24 times a sol (martian day) due to the nature of the orbit of the spacecraft. Ozone is retrieved within the Hartley Band between wavelengths $240-320\,nm$, while water ice is retrieved using five diffraction orders which range between $2.2\,\mu m$ and $4.3\,\mu m$. See M. R. Patel et al. (2021) and Liuzzi et al. (2020) for the full retrieval process for ozone and water ice respectively.

2.2 Vertical Cross-Correlation

We conduct a cross-correlation between ozone and water ice vertical profiles retrieved from the NOMAD instrument to assess the vertical relationship between the two species. In terrestrial studies, this technique is often used between two time series to determine whether there is a correlated time lag between the variables, along with the nature of this time displacement (e.g. Arattano and Marchi (2005); Peppa et al. (2017)). It is often used when one variable is expected to influence the other and there may be a delay in the response. By displacing the altitude, any vertically displaced patterns between the ozone and water ice can be identified, which, due to the suppression of HO_x in water-ice clouds, may impact ozone at different altitudes. In addition, water-ice clouds can span several kilometres and, with a standard Pearson's correlation, any increase in ozone which does not span the full altitude range of the water-ice cloud would not be consistently detected. By conducting a cross-correlation, any variation in ozone within the water-ice cloud may be detected within a few kilometres displacement. Furthermore, a standard correlation may not detect any relationship if the vertical profiles of water ice and ozone are displaced at differing altitudes due to any interpolation error, while the cross-correlation is able to capture this with the vertical lag.

Each cross-correlation conducted on a pair of vertical profiles produces multiple correlations at different altitude displacements. In this study, a 2-tailed Student's T-test is used to assess the p-value of each correlation at a significance level of 5% and, from all the significant correlations, the one with the lowest p-value is selected as the most significant correlation. The p-value is the probability of a result being at least as extreme as the observed datapoint, with the assumption that the null hypothesis is true. In this analysis, it is the probability of obtaining a correlation at least as extreme as the observed

Table 1. Total number of vertical profiles for high northern and southern latitudes, followed by the number of profiles which both have at least 1 ppmv of water ice, 0.03 ppmv of ozone, and a minimum of 6 datapoints in each profile. Positive correlations are only included if the altitude displacement is within ± 10 km.

Latitude (°)	Total Profiles	Profiles used	Positive correlations	Percentage positive
$\geq$ 45 N	383	249	90	36.1%
$\geq$ 45 S	711	564	314	55.7%

correlation between ozone and water ice, given the assumption that there is no vertical correlation between ozone and water ice.

Profiles with no variation and very low volume mixing ratios (vmr) are unsuitable for the vertical correlation analysis as they can produce false correlations that would obscure results in the rest of the analysis. Including such profiles may return positive correlations between ozone and water ice, which have no physical meaning as the vmr is so low. As a result, a minimum condition of at least one value in each ozone profile exceeding a threshold of 0.03 ppmv is set. This restriction enables the vertical variation of ozone in regions of low abundance (such as in the northern hemisphere) to be included in the analysis. Panel (b) of Figure 1 shows the ozone vertical profiles $> 45°$ N for L_S $0°$ − $180°$ MY 35. Panels (c) and (d) show the vertical profiles of water ice and water vapour respectively at the same times and locations, while panel (a) gives the corresponding latitude and local time of the profile. Panels (e), (f), (g), and h show the same species but for $> 45°$ S. Similarly, a minimum threshold of at least one value in each water ice profile exceeding 1 ppmv is used. These values are defined graphically and the sensitivity analysis undertaken indicated that the number of profiles retained for the analysis were robust for the threshold (see Supplementary Information for the sensitivity analysis). In addition, a threshold of a minimum of 6 datapoints in each profile is used to filter profiles with poor vertical coverage and which otherwise would be unsuitable for the cross-correlation analysis and lead to insignificant correlations.

Figure 2 shows an example of the cross-correlation on a pair of profiles; the maximum correlation between the profiles occurs when the ozone is 4 km above the water ice (red cross on right panel; correlation 0.85). This corresponds to the increase in ozone between $34-28$ km, peaking at 0.45 ppmv matching with the increase in water ice between $31-25$ km which peaks at 7.0 ppmv (left panel). At an altitude displacement $<$ -10 km the decrease in ozone from the peak between $28-24$ km matches with the decrease in water ice which occurs from $25 - 10$ km, causing the correlation at this displacement to increase to 0.8. See the Supplementary Information for further details on the methodology used to calculate the cross-correlation and filter data.

2.3 1-D Model

The 1-D model used in this work (henceforth referred to as the 1-dimensional Martian Photochemical Model, 1-D MPM) is derived from the Open University modelling Group Mars GCM (MGCM), which exists as a collaboration between the Laboratoire de Météorologie Dynamique (LMD), the Open University, the University of Oxford, and Instituto de Astrofísica de Andalućia (Forget et al., 1999).

By using a 1-D model, the interactions between tracers can be identified purely as chemical interactions without the added complexity of a 3-D dynamical model, such as the transport of heat, chemical species, and aerosols. The effects of heterogeneous re-
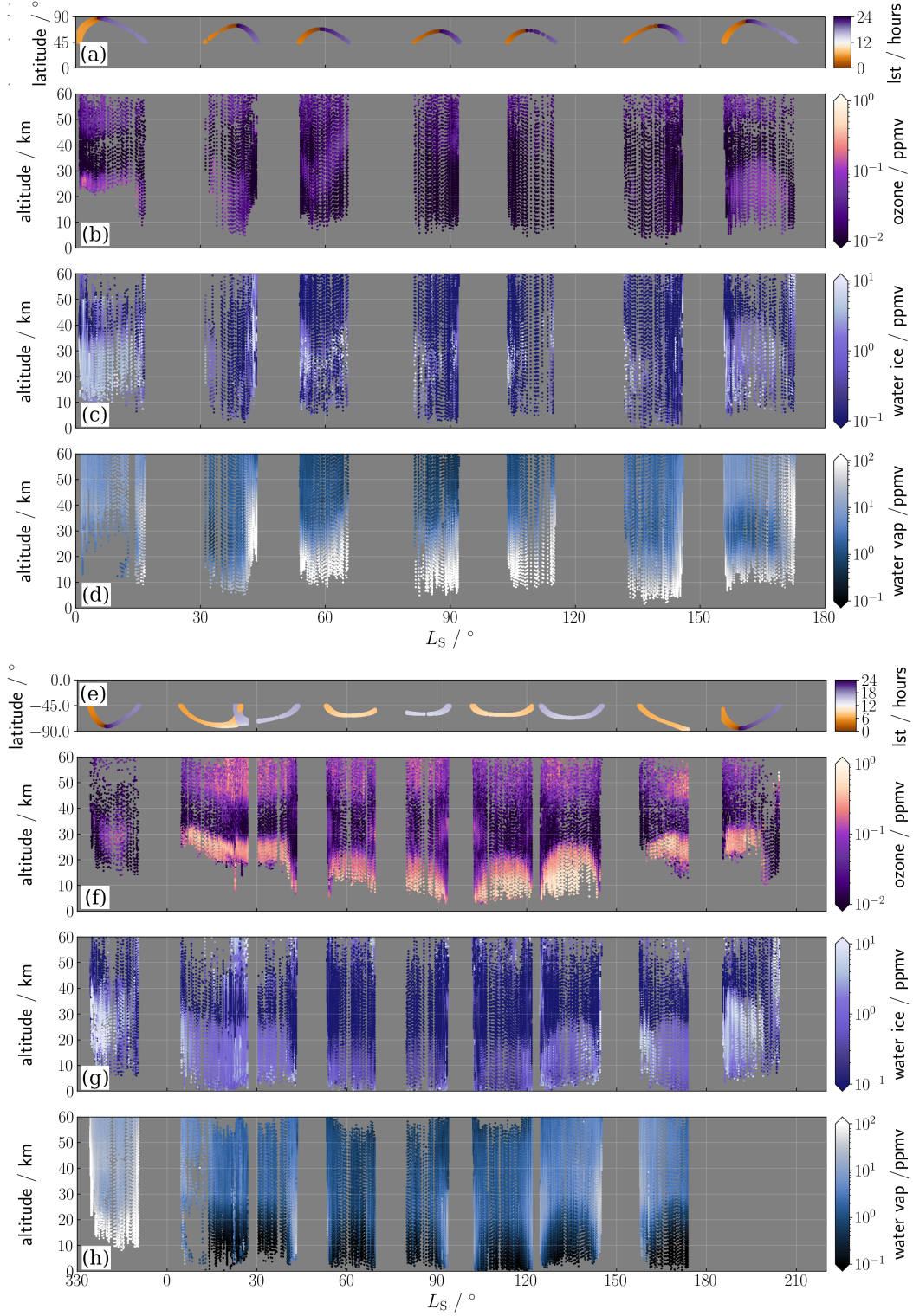
Figure 1. (a) The latitude and local time at which each observed profile is taken. Vertical profiles at high northern latitudes ($> 45°$ N) of (b) ozone (M. R. Patel et al., 2021); (c) water ice (Liuzzi et al., 2020); and (d) water vapour (Villanueva et al., 2022) from $L_S = 0° - 180°$ MY 35 from the NOMAD instrument. (e), (f), (g) and (h); equivalent as above but for high southern latitudes ($> 45°$ S).
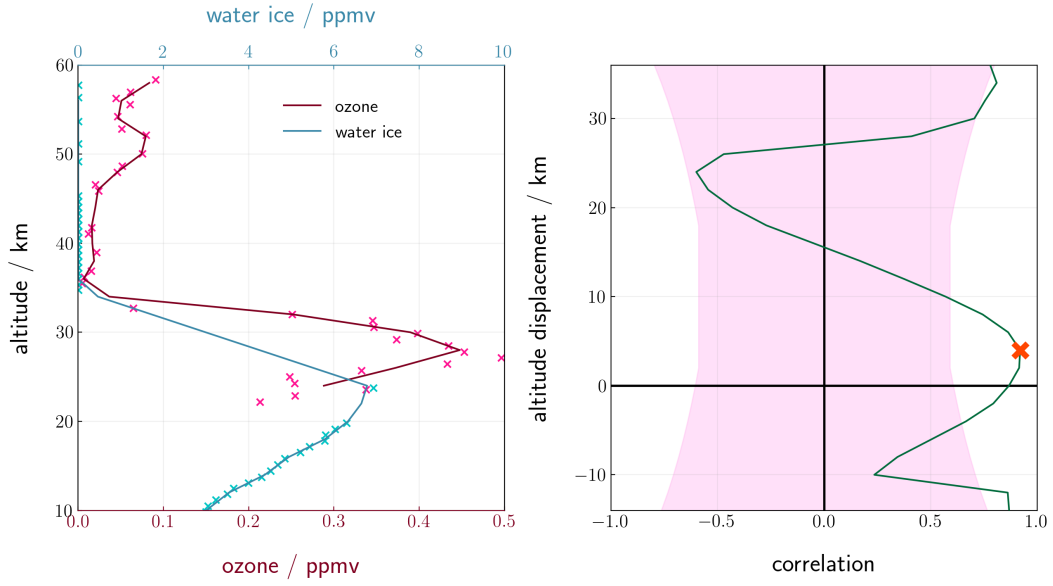
Figure 2. An example of a cross-correlation analysis between a pair of profiles: (left panel) vertical profiles of (blue) water ice; and (red) ozone, where the crosses are the datapoints and the lines are the interpolated profiles every 2 km: (right panel) the (green) vertical correlation between the profiles across all displacements. A positive displacement of 4 km corresponds to a shifting of the water ice profile up by 4 km. The pink area marks the correlations which are not significant according to a Student's T-test at 5% significance. The red cross indicates the most significant vertical correlation of the cross-correlation. Profiles are from NOMAD/TGO at $L_\mathrm{S} = 187°$, latitude 70.5° S, 2020.04.21 11:04:57 UTC.

actions on ozone can therefore be isolated and, by running the model both with and without the heterogeneous reactions, the difference between ozone in both scenarios highlights the direct impact of heterogeneous chemistry on ozone.

The 1-D MPM is compiled with 70 levels, spaced non-linearly according to pressure, with 22 tracers and 60 chemical and photochemical reactions. Initial starting conditions are taken from the outputs of the MGCM, run with data assimilation of temperature and dust retrievals (J. A. Holmes et al., 2020) from the Mars Climate Sounder (MCS) instrument aboard the Mars Reconnaissance Orbiter, with photochemistry and the new ASIS chemical scheme. The heterogeneous chemical scheme, originally taken from Lefèvre et al. (2021), has been updated to improve the representation of heterogeneous chemistry. The products of the improved heterogeneous reactions are treated as a separate species rather than recycled into water vapour and oxygen. The improved scheme also includes a third heterogeneous reaction using H_2O_2 (Pouvesle et al., 2010). The OH, HO_2 and H_2O_2 are converted into three separate species which are unable to react in any way aside from converting back to their original species. In this heterogeneous scheme, water ice is treated as a sink for HO_x. For OH, this is represented by,

$$OH + ice \rightarrow ice_{OH}, \tag{1}$$

where ice_{OH} is the added species, representing a 'sink' for the OH which is adsorbed onto water-ice particles. The concentration of the ice_{HOx} (and $ice_{H_2O_2}$) species only decreases when either the tendency of water ice (the rate of change from the previous timestep) is negative and thus water ice sublimates to water vapour or if the water ice abundance is 0.

Unlike for OH and HO_2, the adsorption of H_2O_2 onto water ice is a reversible reaction (Pouvesle et al., 2010). The Langmuir adsorption model explains the reversible reaction of the adsorption of species on a monolayer surface. Therefore, the Langmuir reaction rate, which has been derived from laboratory experiments, is used for the heterogeneous reaction rate of H_2O_2 in the model:

$$\theta_A = \frac{K_{eq}^A \, p_A}{1 + K_{eq}^A \, p_A}, \tag{2}$$

where p_A is the partial pressure of the species (e.g. HO_x), K_{eq}^A is the equilibrium constant of the reaction, and θ_A is the fractional coverage, or the ratio between the volume of gas adsorbed onto the surface to the volume of gas adsorbed onto the surface at maximum occupancy, assuming only monolayer of adsorbate onto the surface (Langmuir, 1918).

Figure 3 shows the vertical profile of ozone for the previous and new heterogeneous schemes and the differences between them over one sol (note the non-linearity on the difference colourbar on the bottom panel). At lower altitudes < 25 km there is little difference in ozone abundance between the simulations (indicated by the pale green in the bottom panel). However, at higher altitudes, the new heterogeneous scheme simulates a lower ozone abundance throughout the sol, between 30–55 km (red in the bottom panel). This is likely due to the water ice, which formed at a uniform concentration between 30–50 km throughout the sol in both simulations (not shown). During the day (between 0600–1800 hours), ozone abundance in the new scheme gradually increases up to 0.1 ppmv, and the altitude range it spans also increases from 30–40 km to 30–60 km (top panel). In contrast, ozone has little variation during the day in the old heterogeneous scheme, and has a higher abundance (0.1 ppmv between 0600–1800 hours), which ranges between 30–45 km. The greatest difference between the two schemes occurs at nighttime, where the ozone abundance in the new scheme increases to 0.8 ppmv around 50 km, while in the old scheme,
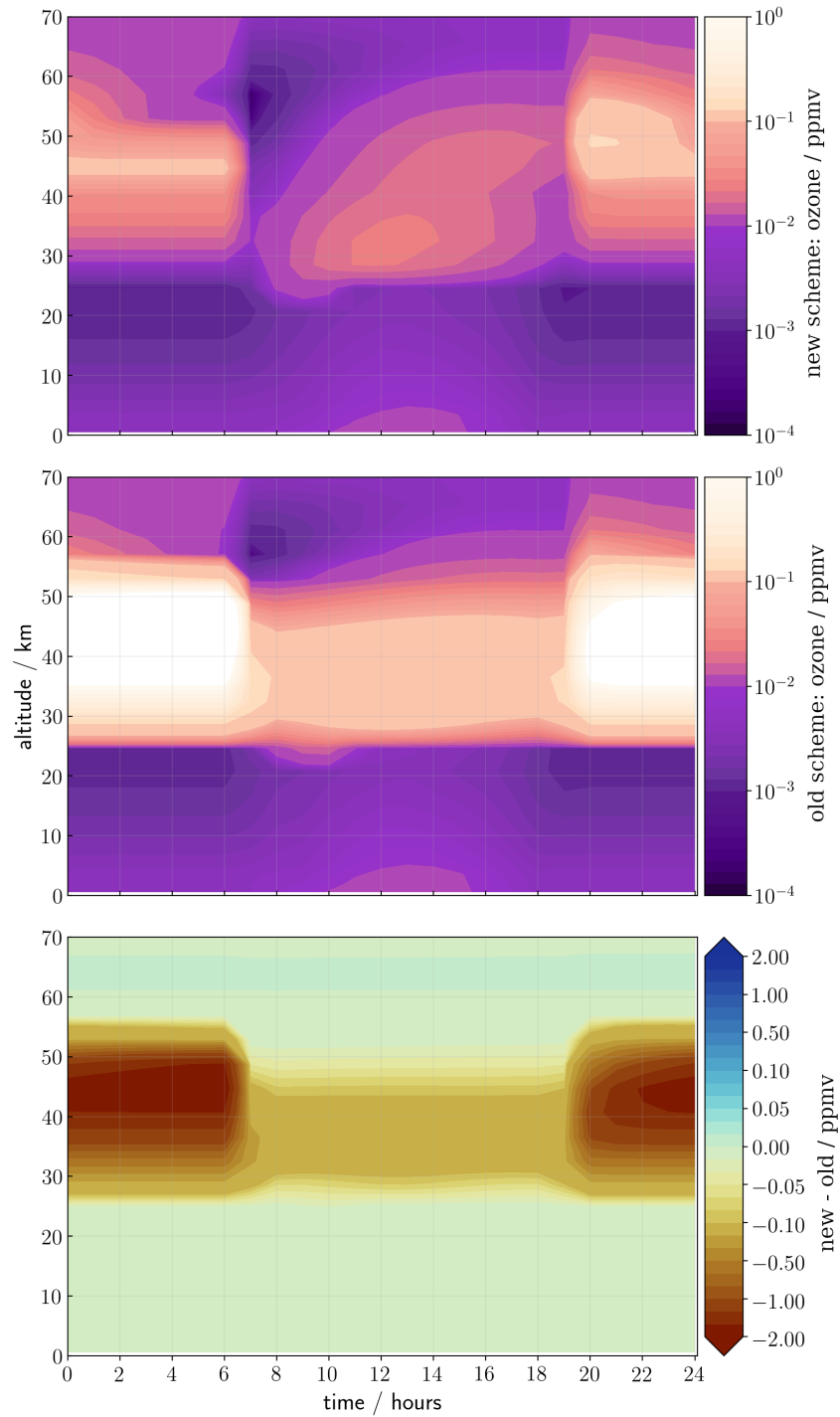
Figure 3. Simulation of ozone abundance over a sol at $0°\,S$, $L_S = 15°$ with the 1-D MPM using; (top) the new heterogeneous chemistry scheme; (middle) the old heterogeneous chemistry, and (bottom) the difference between the two.

ozone increases to > 2 ppmv between 30–50 km. Overall, the new heterogeneous scheme has a lower ozone total column abundance, due to the differences > 30 km.

Two scenarios with a high and low water vapour abundance are simulated with the 1-D MPM to represent high northern and southern latitudes respectively; the scenarios are a simplified representation of high latitude regions and longer temporal periods during the aphelion season. To reduce the parameter differences between the high and low water vapour scenarios, the latitudes and local times are kept consistent at latitude $0°$ and 1200 local solar time (LST); only the time of year is changed, with the low and high water vapour scenario at $L_S = 60°$ and $L_S = 180°$ respectively. By varying the L_S, the solar insolation decreases in the $L_S = 60°$ simulation and results in a lower water vapour abundance due to lower temperatures. The vertical structure of temperature remains similar in both scenarios due to the same latitude used, and the local solar time ensures it is a photochemically active part of the day. This results in the water-ice clouds form at similar altitudes in both scenarios.

Despite the vertical profiles covering high latitudes, the model scenarios are used only to investigate the ozone variation under different water vapour abundance and not the latitudes themselves. Due to the limitations in the condensation scheme of the model, it is not appropriate to run the 1D-MPM at high latitudes, and thus only low latitudes are used in this study. For verification, the 1-D MPM was run at different L_S, local time, and latitudes to investigate the chemical response of ozone from the heterogeneous reactions. The two scenarios used in this study produce similar results to the other simulations and are representative of the ozone variation (not shown). The results from these runs were verified against the MGCM from J. Holmes et al. (2021) and the JPL Caltech 1-D model from Viúdez-Moreiras et al. (2019) and found to be in good agreement (see Supplementary Information for a full comparison).

The model is run both with and without heterogeneous chemistry, with the gas-phase only simulation used as a control to investigate the chemical impacts from the heterogeneous reactions. Further details of the adapted heterogeneous chemistry parameters of the model are in the Supplementary Information.

3 Results

The two high latitude regions ($> 45°$ N/S) used in this study cover $L_S = 0° - 180°$ MY 35 and have contrasting abundances of water vapour. The time period incorporates the northern spring equinox to the northern autumnal equinox, where, from previous studies, ozone is underpredicted. Figure 4 shows the averaged water ice profiles $> 45°$ S between $L_S = 100° - 120°$ and the ozone difference between modelled and observed profiles. An ozone difference greater than 0 ppmv (dark red bars) indicates an underprediction in the MGCM, which follows a similar trend to the water ice abundance. The greatest ozone deficit occurs at lower altitudes (< 20 km) and coincides with a higher water ice concentration, while a small deficit occurs above 40 km. Figure 4 is representative of the relationship between the ozone deficit and water ice present throughout the southern hemisphere from $L_S = 0° - 180°$ (not shown).

During northern summer, the water ice cap melts, leading to a high abundance of water vapour in the northern hemisphere (Clancy & Nair, 1996; Montmessin & Lefèvre, 2013; Steele et al., 2014). Using the observed vertical profiles from NOMAD between $10 - 50$ km, the total water vapour abundance is, on average, one magnitude larger in the northern hemisphere than the southern (1.37×10^{-2} pr-μm compared to 1.78×10^{-3} pr-μm) [From Geronimo 2022]. Note that not all occultations extend to the surface, and thus the calculated total column abundance only extends down to 10 km. This is demonstrated in panel (d), Figure 1, where between $L_S = 30° - 180°$ the water vapour reaches concentrations > 100 ppmv at 30 km and below. The total column of water vapour is there-
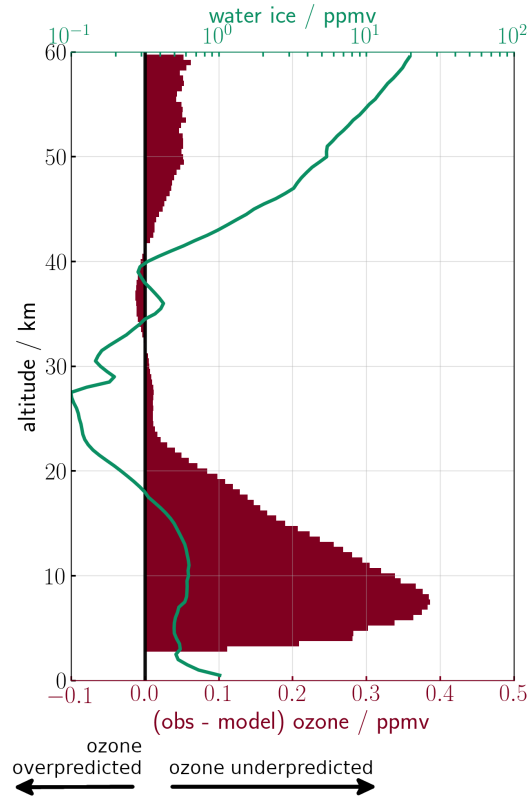
Figure 4. Averaged profiles (212 vertical profiles) > 45° S between $L_S = 100° - 120°$ of (green line) observed water ice, and (red bars) the difference in ozone (observed – modelled). Positive values indicate an underprediction of ozone. Modelled data are taken from the MGCM, assimilated with temperature and dust retrievals from MCS.
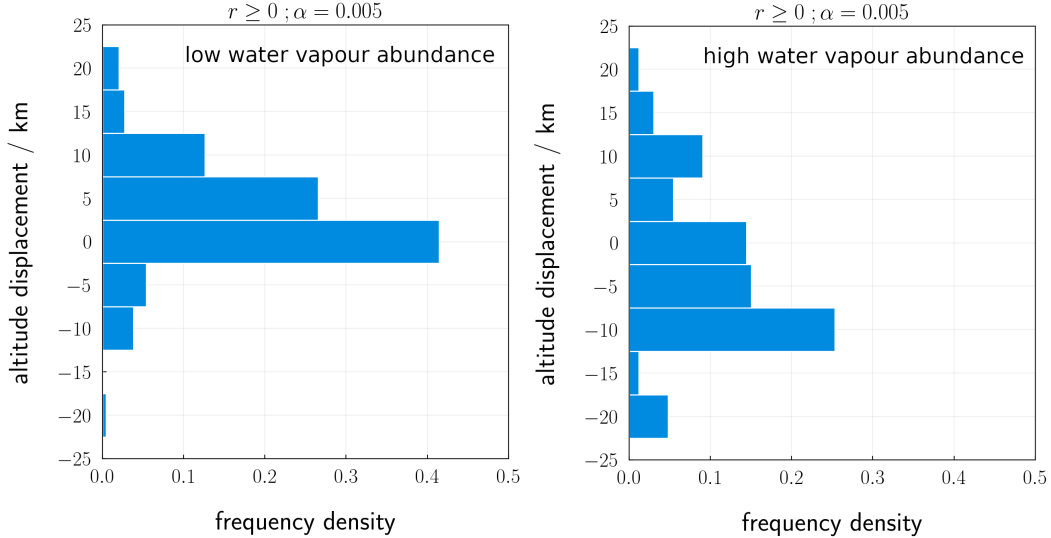
Figure 5. Histogram of altitude displacements for significant, positive, vertical correlations between ozone and water ice observed profiles for (left) southern latitudes ($> 45°$ S) $L_S = 0° - 180°$ and (right) northern latitudes ($> 45°$ N) between $L_S = 30° - 180°$. α shows the significance level, and $r \geq 0$ indicates positive correlations only. Bins cover $5\,\mathrm{km}$, with the y axis label denoting the centre of the bin (e.g. the $0\,\mathrm{km}$ bin includes values from $2.5\,\mathrm{km}$ to $2.5\,\mathrm{km}$.)

fore likely much higher, as the lowest altitudes have the greatest contribution to the total column measurement.

3.1 Low Vapour Case: Ozone – Water Ice Relationship

The results from cross-correlation between the ozone and water ice vertical profiles in the southern latitude region suggest there are significant, positive vertical correlations when the ozone and water ice profiles match at the same altitudes. The absence of high abundances of water vapour in the southern hemisphere allows the relationship between ozone and water ice to be seen without interference from the presence of water vapour. The cross-correlation results demonstrate a clear relationship between ozone and water ice within a vertical displacement range of $\pm 10\,\mathrm{km}$ of the two species; the left panel of Figure 5 shows a histogram of the altitude displacement from the most significant positive correlations of each profile pair in the southern latitude region. An altitude displacement of $4\,\mathrm{km}$ indicates a positive shift in the water ice profile from its original position by $4\,\mathrm{km}$, and thus indicates that the water ice profile matches with an ozone profile which is $4\,\mathrm{km}$ above. An altitude displacements of $0\,\mathrm{km}$ implies a correlation between the two species at their original position.

In the histogram, there is a sharp peak between $-2.5 - 2.5\,\mathrm{km}$ with a frequency density of 0.41, implying that water ice and ozone profiles correlate strongly at the same altitude, or when there is a small altitude displacement ($< 2.5\,\mathrm{km}$). Table 1 shows the number of profiles used in the analysis and the percentage of profiles which have positive correlations within $\pm 10\,\mathrm{km}$. Of the profiles suitable for cross-correlation, 55.7% of the most significant correlations are positive within this altitude range.

The positive correlation between ozone and water ice is continuous throughout the season can be seen visually in panels (f) and (g) in Figure 1. Both species follow a sim-
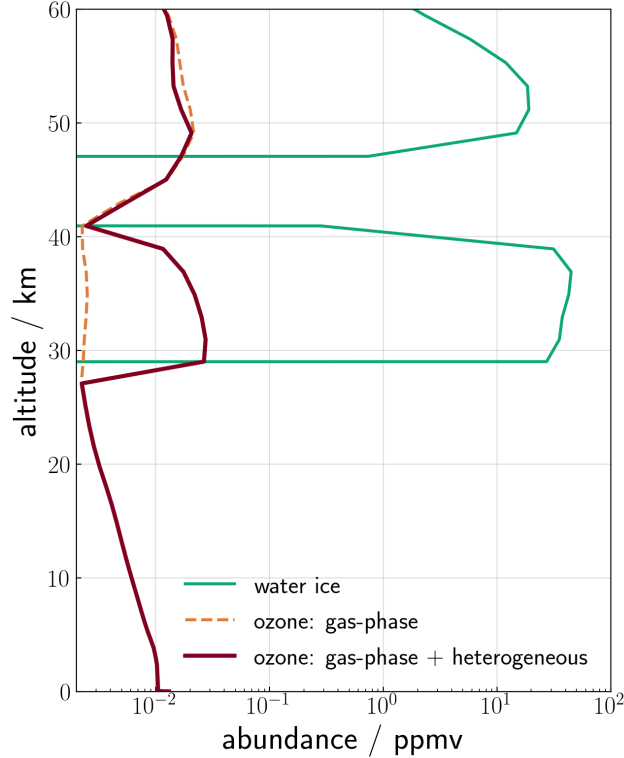
Figure 6. A single modelled vertical profile from the 1-D MPM of (dark red) ozone from the heterogeneous run, (dashed orange) ozone from gas-phase only run and (green) water ice. Profiles are simulated at 1200 LST, latitude $0°$, $L_S = 0°$.

376 ilar latitudinal trend with abundances ranging between 0.2–1 ppmv for ozone and 0.5–
377 3 ppmv for water ice between 0–30 km. The cross-correlation matches the variation in
378 ozone and water ice profiles together at 0 km displacement, as both species have a sim-
379 ilar vertical variation. In panels (f) and (g) of Figure 1, both the water ice and ozone
380 have increased abundances below 30 km, which decrease above this altitude.

381 During this period, the water vapour abundance is low due to the cold atmospheric
382 temperatures during southern winter. Panel (h) of Figure 1 shows the vertical profiles
383 of water vapour derived from NOMAD observations from (Villanueva et al., 2022); the
384 water vapour ranges from < 0.1 ppmv to 30 ppmv, with much of the water vapour only
385 observed at altitudes above 30 km.

386 Figure 6 shows a modelled profile from the 1-D MPM both with and without het-
387 erogeneous chemistry taken at 1200 LST, $L_S = 0°$, latitude $0°$ as explained in Section 2.
388 Between $30-40$ km there is an increase in ozone in the heterogeneous simulation (dark
389 red) which is not observed in the gas-phase-only simulated ozone (dashed orange). This
390 increase is due to the heterogeneous reactions which occur when water ice (green) is present.
391 The water ice adsorbs the HO_x and reduces the HO_x abundance, which results in a lower
392 ozone destruction rate and enhances the ozone abundance. The peak increase in ozone
393 from heterogeneous reactions in the low water vapour abundance simulations are pro-
394 portional to $43-75\%$ of the peak ozone deficit shown in Figure 4.

395 The ozone simulated with heterogeneous chemistry between $50-60$ km does not
396 exhibit the same response, however, despite the formation of water ice at these altitudes.
397 Indeed, the ozone simulated with heterogeneous chemistry is slightly lower than the gas-

phase-only ozone. This is due to a decrease in water ice abundance between $50-60$ km from the previous timestep, which causes the release of previously adsorbed hydroxyl radicals, increasing their abundance compared to the control (gas-phase-only) simulation.

3.2 High Vapour Case: No Ozone – Water Ice Correlation

Given that we have found that the altitude displacement between ozone and water ice is likely with ± 10 km altitude range in the southern hemisphere, exploring the correlation between ozon and water ice in the northern hemisphere at this altitude range could yield similar results. The right panel of Figure 5 shows the histogram of significant, positive vertical correlations for observed ozone and water ice profiles at high northern latitudes. Unlike in the southern hemisphere, the distribution of altitude displacements in the northern hemisphere is more uniform and there is no clear correlation between ozone and water ice in one altitude displacement range. In addition to this, there are proportionally fewer significant positive correlations, with only 36.1% of the most significant correlations being positive within ± 10 km displacement, compared to 55.7% in the southern latitude region (see Table 1).

As discussed previously, the high northern latitudes between $L_S = 30°-180°$ have a higher water vapour abundance than the high southern latitudes (lower panels of Figure 1), as the time period covers the northern summer and the sublimation of the water-ice cap (Montmessin & Lefèvre, 2013; Steele et al., 2014). To simulate similar conditions of higher water vapour abundance, a 1-D MPM simulation at latitude 0°, $L_S = 180°$ is used to investigate the response of ozone to the heterogeneous reactions. The vertical profile from this model run is then compared to another with a much lower water vapour abundance at $L_S = 60°$; total column water vapour abundance is 9.3 pr-μm and 3.8 pr-μm for the high and low vapour scenarios respectively. Note that these values are the total column abundance for the full vertical column and thus not directly comparable to the abundances calculated for the observed vertical profiles which only include altitudes between 10–50 km. The total column water vapour abundances between $10-50$ km are 2.1 pr-μm and 0.008 pr-μm for the high and low water vapour scenario respectively.

Figure 7 demonstrates the impact of heterogeneous chemistry on ozone abundance for low ($L_S = 60°$; panels (a) and (b)), and high ($L_S = 180°$; panels (c) and (d)) water vapour abundances through the change in hydroxyl radicals. Panels (a) and (c) show the vertical profile of water ice and water vapour (lines) as well as the ozone residual (bars) which is the heterogeneous simulation minus the gas-phase simulation. Panels (b) and (d) shows the vertical profile of ozone and HO_x (combined OH + HO_2). Panel (a) shows an excess of ozone (dark red bars) from the heterogeneous simulation up to 0.05 ppmv in the low water vapour scenario (shown by the water vapour profile; dark blue) between 25–40 km. Panel (b) shows the ozone (dark red) and HO_x (OH and HO_2; orange) abundance for the control (solid) and heterogeneous (dashed) simulation; the large difference between the two HO_x abundances (over two orders of magnitude difference between $25-30$ km) is a direct result of the heterogeneous reactions caused by the presence of water ice at these altitudes. In contrast, panel (c) only has an ozone residual of up to 0.005 ppmv in the high water vapour abundance scenario despite having a larger water ice abundance (light blue) of 30 ppmv compared to 10 ppmv. The HO_x abundance is over an order of magnitude higher in the control simulation between 30–45 km and the adsorption of HO_x onto water ice is proportionally much smaller than the lower water vapour scenario; between 30–35 km, HO_x decreases from 3×10^{-3} to 1×10^{-3} ppmv, while in the low vapour scenario HO_x decreases from 3×10^{-4} to 1×10^{-5} ppmv despite the water ice abundance being three times less.
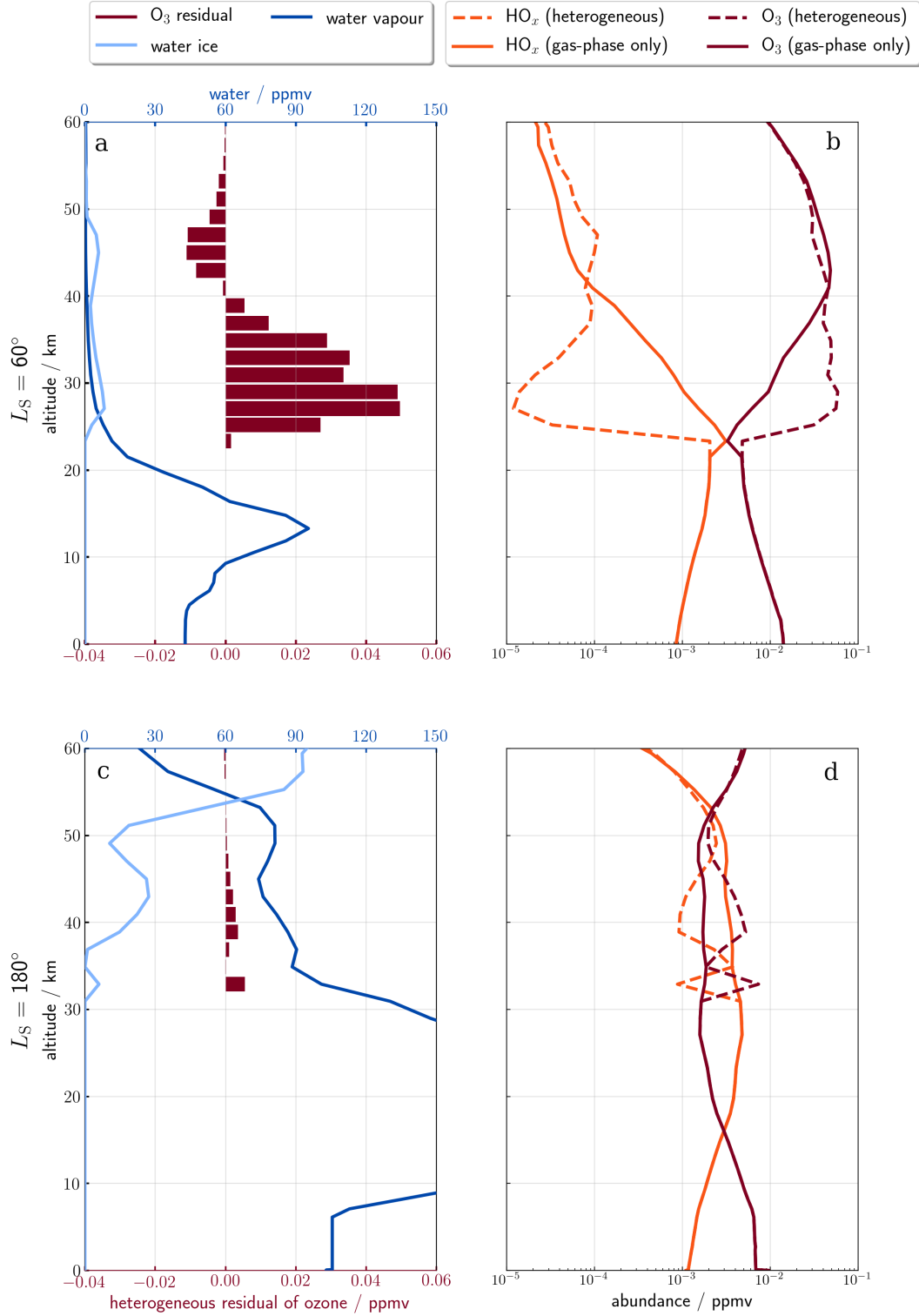
Figure 7. Modelled profiles from the 1-D MPM of (a and b) low water vapour (at $L_S = 60°$), and (c and d) high water vapour (at $L_S = 180°$) at latitude 0°, local solar time 1200 hours. (First column; (a) and (c)) vertical profiles of (light blue) water ice, (dark blue) water vapour, and (dark red bars) the ozone residual (calculated by subtracting the heterogeneous ozone from the gas-phase only ozone). Abundance difference for ozone is on the bottom x-axis and abundance for water ice and vapour is on the top x-axis. (Second column; (b) and (d)) vertical profiles of (dark red) ozone and (orange) HO_x for (dashed) heterogeneous and (solid) gas-phase-only simulations. Note the abundances are on a logarithmic scale.

4 Discussion

4.1 Impact of Heterogeneous Chemistry on Ozone

The positive vertical correlation between ozone and water ice in the southern latitude region can be used as a proxy for the presence of heterogeneous reactions. The results of the correlation analysis are supported by the 1-D MPM simulations which, in Figure 6, demonstrate the difference between ozone profiles in the presence of water ice, both with and without heterogeneous chemistry. The increase in ozone vmr due to heterogeneous reactions occurs at the same altitudes water ice is present in. According to the simulated profile in Figure 6, this is between $30 - 40 \, \text{km}$.

The increase in ozone vmr due to heterogeneous reactions occurs at the same altitudes as water ice is present, which, in the simulated profile in Figure 6, is between 30–$40 \, \text{km}$. The heterogeneous reactions act as a sink for HO_x, reducing the abundance of HO_x as the water-ice surface area increases. As HO_x reactions with ozone are one of the main destructive pathways of ozone, the decrease in HO_x vmr ultimately leads to an increase in ozone vmr within the altitudes that water ice has formed.

The adsorption rate of heterogeneous reactions is dependent on the water-ice surface area, HO_x molecular density, and temperature. At higher altitudes, all three factors are typically lower due to the exponential decrease in pressure and general decrease in temperature. The impact of heterogeneous chemistry, therefore, is reduced at higher altitudes. The decrease in molecular density of HO_x with increasing altitude results in a smaller difference between the simulations, with and without heterogeneous chemistry; this is shown by the decrease in difference of ozone, as altitude increases in Figures 6 and 7. This suggests that heterogeneous chemistry has less influence on the ozone abundance at high ($> 50 \, \text{km}$) altitudes, which is reflected in the ozone deficit between simulated and observed vertical profiles as seen in Figure 4. The largest ozone deficit between simulated and observed profiles coincides with a higher water ice concentration below $30 \, \text{km}$, while only a small deficit occurs above $40 \, \text{km}$. The positive vertical correlation between ozone and water ice occurs below $30 \, \text{km}$; this relationship matches the response observed in the 1-D MPM heterogeneous simulation, in which ozone increases at the same altitudes water ice forms. Heterogeneous chemistry could therefore explain some $(43-75\%)$ of the ozone deficit, as the addition of the heterogeneous reactions increases ozone at the altitudes water ice is present and has a greater impact on ozone abundance at low altitudes. As the heterogeneous reactions do not fully account for the ozone deficit, it is possible that there are other unknown reactions occurring, or the rates of the heterogeneous reactions themselves may be incomplete.

4.2 Water Vapour Influence on Heterogeneous Chemistry

The lack of any positive vertical correlation between ozone and water ice at a consistent altitude range in the northern hemisphere suggests there is no relationship between ozone and water ice and, by proxy, no heterogeneous chemistry present. This conflicts with the clear relationship observed between the two species in the southern hemisphere.

One suggestion for this could be that, globally, there is no heterogeneous chemistry occurring and the relationship observed in the southern hemisphere is simply an anti-correlation between ozone and water vapour portrayed through the water ice distribution which, itself, appears to be an inverse of the water vapour distribution (Figure 1). If this were the case, however, the relationship observed in the northern hemisphere should be similar to that of the southern hemisphere.

These contrasting results between the high northern and southern latitudes therefore require an additional explanation. The 1-D MPM simulations of a high and low wa-

ter vapour scenario enable an explicit investigation into the chemical impact of the heterogeneous reactions between HO_x and ozone. Despite the decrease in HO_x abundance from the control to the heterogeneous simulation in the high water vapour scenario (lower panels, Figure 7), there is little difference in ozone abundance, indicating that the heterogeneous reactions have relatively little impact on ozone abundance in circumstances of high HO_x abundance. As HO_x is a by-product of water vapour photolysis, a high abundance of water vapour can be assumed proportional to a high HO_x abundance. In the northern hemisphere during northern summer, the water vapour abundance is higher than observed in the southern hemisphere and, by extension, the HO_x abundance is also likely to be greater. The relative decrease of HO_x abundance as a result of heterogeneous chemistry has a negligible impact on the abundance of ozone and is unlikely to be detectable through ozone variation. Therefore, ozone and water ice would not be expected to have a positive relationship in scenarios of high water vapour abundance, as heterogeneous chemistry is offset by the additional availability of HO_x and the ozone abundance does not significantly increase under such circumstances.

4.3 Conclusions

We find that the influence of heterogeneous reactions on ozone is dependent on the abundance of water vapour, which undergoes seasonal and spatial variation. The relationship between the observed ozone and water ice, which is used as a proxy for heterogeneous chemistry, is also expected to vary temporally and spatially.

In the cross-correlation analysis at high southern latitudes, there is a positive vertical correlation between ozone and water ice at 0 km displacement. In contrast, in the northern latitudes, when there is a much higher water vapour abundance, there is no clear positive correlation. In the 1-D MPM simulations, the ozone abundance is much lower in the high water vapour scenario and the ozone residual between the heterogeneous and gas-phase simulation is closer to 0 ppmv, implying that there is a minimal effect (< 0.005 ppmv increase) of heterogeneous chemistry on ozone under high water vapour conditions.

The photolysis of water vapour is not the sole factor in the water cycle affecting the global ozone distribution — water ice also appears to influence ozone abundance indirectly through the adsorption of hydroxyl radicals.

The cross-correlation conducted on the ozone and water ice vmr profiles shows that these two variables are positively correlated in the vertical. This is contrary to previous studies which found an anti-correlation between the total abundance of ozone and water ice (Clancy et al., 2016). From investigating the ozone variation between 1-D MPM outputs with and without heterogeneous chemistry, we show that heterogeneous reactions between HO_x and water ice are a plausible explanation for the positive vertical correlation between ozone and water ice.

Furthermore, heterogeneous chemistry increases the ozone vmr at altitudes water ice forms, and thus could explain some of the ozone deficit in GCMs when compared to observations, which is in agreement with Lefèvre et al. (2008, 2021). While the addition of heterogeneous chemistry may not fully resolve the ozone deficit seen in GCMs, it increases the ozone abundance at locations which currently underpredict ozone, while having a minimal effect on ozone at higher altitudes and in areas of higher water vapour abundance (< 0.005 ppmv), where models already show good agreement with observations.

Heterogeneous chemistry affects the variation in hydroxyl radicals. Therefore, establishing the nature of heterogeneous reactions is important in understanding the variation in hydroxyl radicals, which themselves are crucial to the stability of the atmosphere e.g. McElroy and Donahue (1972); Clancy and Nair (1996). The presence of water-ice clouds could indirectly affect the recombination of carbon monoxide and molecular oxygen, which is catalysed by hydroxyl radicals. Future work could include establishing the

full spatial and temporal impact of heterogeneous chemistry on ozone and hydroxyl radicals by implementing the improved chemical scheme into a 3-D model, as well as investigating how the change in HO_x in water-ice clouds could impact other species aside from ozone.

Acknowledgments

References

Anbar, A., Leu, M.-T., Nair, H., & Yung, Y. (1993). Adsorption of ho$_x$ on aerosol surfaces: Implications for the atmosphere of mars. *Journal of Geophysical Research: Planets*, *98*(E6), 10933–10940.

Arattano, M., & Marchi, L. (2005). Measurements of debris flow velocity through cross-correlation of instrumentation data. *Natural Hazards and Earth System Sciences*, *5*(1), 137–142. Retrieved from https://nhess.copernicus.org/articles/5/137/2005/ doi: 10.5194/nhess-5-137-2005

Barth, C. A., Hord, C. W., Stewart, A. I., Lane, A. L., Dick, M. L., & Anderson, G. P. (1973). Mariner 9 ultraviolet spectrometer experiment: Seasonal variation of ozone on mars [Journal Article]. *Science*, *179*(4075), 795-796. Retrieved from http://science.sciencemag.org/content/sci/179/4075/795.full.pdfhttp://science.sciencemag.org/content/179/4075/795.long doi: 10.1126/science.179.4075.795

Bell III, J. F., Wolff, M. J., Malin, M. C., Calvin, W. M., Cantor, B. A., Caplinger, M. A., ... Thomas, P. C. (2009). Mars reconnaissance orbiter mars color imager (marci): Instrument description, calibration, and performance. *Journal of Geophysical Research: Planets*, *114*(E8). Retrieved from https://agupubs.onlinelibrary.wiley.com/doi/abs/10.1029/2008JE003315 doi: 10.1029/2008JE003315

Benson, J. L., Kass, D. M., & Kleinböhl, A. (2011). Mars' north polar hood as

observed by the mars climate sounder [Journal Article]. *Journal of Geophysical Research: Planets*, *116*(E3). Retrieved from `https://agupubs` `.onlinelibrary.wiley.com/doi/abs/10.1029/2010JE003693https://` `agupubs.onlinelibrary.wiley.com/doi/pdf/10.1029/2010JE003693` doi: doi:10.1029/2010JE003693

Benson, J. L., Kass, D. M., Kleinböhl, A., McCleese, D. J., Schofield, J. T., & Taylor, F. W. (2010). Mars' south polar hood as observed by the mars climate sounder [Journal Article]. *Journal of Geophysical Research: Planets*, *115*(E12). Retrieved from `https://agupubs.onlinelibrary.wiley.com/doi/abs/` `10.1029/2009JE003554https://agupubs.onlinelibrary.wiley.com/doi/` `pdf/10.1029/2009JE003554` doi: doi:10.1029/2009JE003554

Bertaux, J.-L., Korablev, O., Perrier, S., Quémerais, E., Montmessin, F., Leblanc, F., ... Guibert, S. (2006). Spicam on mars express: Observing modes and overview of uv spectrometer data and scientific results [Journal Article]. *Journal of Geophysical Research: Planets*, *111*(E10). Retrieved from `https://agupubs.onlinelibrary.wiley.com/doi/abs/10.1029/` `2006JE002690https://agupubs.onlinelibrary.wiley.com/doi/pdf/` `10.1029/2006JE002690` doi: doi:10.1029/2006JE002690

Brown, M. A. J., Holmes, J. A., Sellers, G., Liuzzi, G., Lewis, S., & Patel, M. (2022, 4). Dataset: Impacts of heterogeneous chemistry on vertical profiles of martian ozone. Retrieved from `https://ordo.open.ac.uk/articles/dataset/` `Dataset_Impacts_of_Heterogeneous_Chemistry_on_Vertical_Profiles_of` `_Martian_Ozone/19646784` doi: 10.21954/ou.rd.19646784.v1

Cariolle, D., Moinat, P., Teyssèdre, H., Giraud, L., Josse, B., & Lefèvre, F. (2017). Asis v1.0: an adaptive solver for the simulation of atmospheric chemistry. *Geoscientific Model Development*, *10*(4), 1467–1485. Retrieved from `https://gmd.copernicus.org/articles/10/1467/2017/` doi: 10.5194/gmd-10-1467-2017

Clancy, R. T., & Nair, H. (1996). Annual (perihelion-aphelion) cycles in the photochemical behavior of the global mars atmosphere [Journal Article]. *Journal of Geophysical Research: Planets*, *101*(E5), 12785-12790. Retrieved from `https://agupubs.onlinelibrary.wiley.com/doi/abs/10.1029/` `96JE00836https://agupubs.onlinelibrary.wiley.com/doi/pdf/10.1029/` `96JE00836` doi: doi:10.1029/96JE00836

Clancy, R. T., Wolff, M. J., Lefèvre, F., Cantor, B. A., Malin, M. C., & Smith, M. D. (2016). Daily global mapping of mars ozone column abundances with marci uv band imaging [Journal Article]. *Icarus*, *266*, 112-133. Retrieved from `http://www.sciencedirect.com/science/article/pii/S0019103515005266` doi: https://doi.org/10.1016/j.icarus.2015.11.016

Daerden, F., Neary, L., Viscardy, S., Muñoz, A. G., Clancy, R., Smith, M., ... Fedorova, A. (2019). Mars atmospheric chemistry simulations with the gem-mars general circulation model. *Icarus*, *326*, 197 - 224. Retrieved from `http://www.sciencedirect.com/science/article/pii/S0019103518304883` doi: https://doi.org/10.1016/j.icarus.2019.02.030

Forget, F., Hourdin, F., Fournier, R., Hourdin, C., Talagrand, O., Collins, M., ... Huot, J.-P. (1999). Improved general circulation models of the martian atmosphere from the surface to above 80 km. *Journal of Geophysical Research: Planets*, *104*(E10), 24155-24175. Retrieved from `https://` `agupubs.onlinelibrary.wiley.com/doi/abs/10.1029/1999JE001025` doi: https://doi.org/10.1029/1999JE001025

Holmes, J., Lewis, S., Patel, M., Chaffin, M., Cangi, E., Deighan, J., ... Vandaele, A. (2021). Enhanced water loss from the martian atmosphere during a regional-scale dust storm and implications for long-term water loss. *Earth and Planetary Science Letters*, *571*, 117109. Retrieved from `https://` `www.sciencedirect.com/science/article/pii/S0012821X21003642` doi:

https://doi.org/10.1016/j.epsl.2021.117109

Holmes, J. A., Lewis, S. R., & Patel, M. R. (2020). Openmars: A global record of martian weather from 1999 to 2015. *Planetary and Space Science*, *188*, 104962. Retrieved from `https://www.sciencedirect.com/science/article/pii/S0032063319303617` doi: https://doi.org/10.1016/j.pss.2020.104962

Holmes, J. A., Lewis, S. R., Patel, M. R., & Lefèvre, F. (2018). A reanalysis of ozone on mars from assimilation of spicam observations [Journal Article]. *Icarus*, *302*, 308-318. Retrieved from `http://www.sciencedirect.com/science/article/pii/S0019103517302889https://ac.els-cdn.com/S0019103517302889/1-s2.0-S0019103517302889-main.pdf?_tid=22af08de-4263-48e8-8b2a-ec0c20c3647e&acdnat=1539352983_3816efbb662a3bb2f63f199e604ffdd9` doi: https://doi.org/10.1016/j.icarus.2017.11.026

Khayat, A. S. J., Smith, M. D., Wolff, M., Daerden, F., Neary, L., Patel, M. R., ... López-Moreno, J. J. (2021). Exomars tgo/nomad-uvis vertical profiles of ozone: 2. the high-altitude layers of atmospheric ozone. *Journal of Geophysical Research: Planets*, *126*(11), e2021JE006834. Retrieved from `https://agupubs.onlinelibrary.wiley.com/doi/abs/10.1029/2021JE006834` (e2021JE006834 2021JE006834) doi: https://doi.org/10.1029/2021JE006834

Langmuir, I. (1918). The adsorption of gases on plane surfaces of glass, mica and platinum. *Journal of the American Chemical Society*, *40*(9), 1361-1403. Retrieved from `https://doi.org/10.1021/ja02242a004` doi: 10.1021/ja02242a004

Lefèvre, F., Bertaux, J.-L., Clancy, R. T., Encrenaz, T., Fast, K., Forget, F., ... Perrier, S. (2008). Heterogeneous chemistry in the atmosphere of mars [Journal Article]. *Nature*, *454*, 971. Retrieved from `http://dx.doi.org/10.1038/nature07116http://www.nature.com/articles/nature07116` doi: 10.1038/nature07116https://www.nature.com/articles/nature07116# supplementary-information

Lefèvre, F., Lebonnois, S., Montmessin, F., & Forget, F. (2004). Three-dimensional modeling of ozone on mars [Journal Article]. *Journal of Geophysical Research: Planets*, *109*(E7). Retrieved from `https://agupubs.onlinelibrary.wiley.com/doi/abs/10.1029/2004JE002268https://agupubs.onlinelibrary.wiley.com/doi/pdf/10.1029/2004JE002268` doi: doi:10.1029/2004JE002268

Lefèvre, F., Trokhimovskiy, A., Fedorova, A., Baggio, L., Lacombe, G., Määttänen, A., ... Montmessin, F. (2021). Relationship between the ozone and water vapor columns on mars as observed by spicam and calculated by a global climate model. *Journal of Geophysical Research: Planets*, *126*(4), e2021JE006838. Retrieved from `https://agupubs.onlinelibrary.wiley.com/doi/abs/10.1029/2021JE006838` (e2021JE006838 2021JE006838) doi: https://doi.org/10.1029/2021JE006838

Liuzzi, G., Villanueva, G. L., Crismani, M. M., Smith, M. D., Mumma, M. J., Daerden, F., ... Patel, M. R. (2020). Strong variability of martian water ice clouds during dust storms revealed from exomars trace gas orbiter/nomad [Journal Article]. *Journal of Geophysical Research: Planets*, *125*(4), e2019JE006250. Retrieved from `https://agupubs.onlinelibrary.wiley.com/doi/abs/10.1029/2019JE006250` (e2019JE006250 2019JE006250) doi: 10.1029/2019JE006250

McElroy, M. B., & Donahue, T. M. (1972). Stability of the martian atmosphere. *Science*, *177*(4053), 986–988. Retrieved from `http://www.jstor.org/stable/1734144`

Montmessin, F., & Lefèvre, F. (2013). Transport-driven formation of a polar ozone layer on mars [Journal Article]. *Nature Geoscience*, *6*, 930. Retrieved from `http://dx.doi.org/10.1038/ngeo1957http://www.nature.com/`

articles/ngeo1957 doi: 10.1038/ngeo1957https://www.nature.com/articles/ngeo1957#supplementary-information

Nair, H., Allen, M., Anbar, A. D., Yung, Y. L., & Clancy, R. (1994). A photochemical model of the martian atmosphere. *Icarus*, *111*(1), 124 - 150. Retrieved from `http://www.sciencedirect.com/science/article/pii/S0019103584711377` doi: https://doi.org/10.1006/icar.1994.1137

Patel, M., Mason, J., Sellers, G., Holmes, J., & Streeter, P. (2021, 10). NOMAD-UVIS ozone and aerosol vertical profile retrievals for Mars Year 34-35. Retrieved from `https://ordo.open.ac.uk/articles/dataset/NOMAD-UVIS_ozone_vertical_profile_retrievals_for_Mars_Year_34-35/13580336` doi: 10.21954/ou.rd.13580336.v2

Patel, M. R., Antoine, P., Mason, J., Leese, M., Hathi, B., Stevens, A. H., . . . Lopez-Moreno, J. J. (2017). Nomad spectrometer on the exomars trace gas orbiter mission: part 2—design, manufacturing, and testing of the ultraviolet and visible channel [Journal Article]. *Applied Optics*, *56*(10), 2771-2782. Retrieved from `http://ao.osa.org/abstract.cfm?URI=ao-56-10-2771https://www.osapublishing.org/ao/abstract.cfm?uri=ao-56-10-2771` doi: 10.1364/AO.56.002771

Patel, M. R., Sellers, G., Mason, J. P., Holmes, J. A., Brown, M. A. J., Lewis, S. R., . . . Lopez-Moreno, J.-J. (2021). Exomars tgo/nomad-uvis vertical profiles of ozone: 1. seasonal variation and comparison to water. *Journal of Geophysical Research: Planets*, *126*(11), e2021JE006837. Retrieved from `https://agupubs.onlinelibrary.wiley.com/doi/abs/10.1029/2021JE006837` (e2021JE006837 2021JE006837) doi: https://doi.org/10.1029/2021JE006837

Peppa, M. V., Mills, J. P., Moore, P., Miller, P. E., & Chambers, J. E. (2017). Brief communication: Landslide motion from cross correlation of uav-derived morphological attributes. *Natural Hazards and Earth System Sciences*, *17*(12), 2143–2150. Retrieved from `https://nhess.copernicus.org/articles/17/2143/2017/` doi: 10.5194/nhess-17-2143-2017

Perrier, S., Bertaux, J. L., Lefèvre, F., Lebonnois, S., Korablev, O., Fedorova, A., & Montmessin, F. (2006). Global distribution of total ozone on mars from spicam/mex uv measurements [Journal Article]. *Journal of Geophysical Research: Planets*, *111*(E9). Retrieved from `https://agupubs.onlinelibrary.wiley.com/doi/abs/10.1029/2006JE002681` doi: doi:10.1029/2006JE002681

Pouvesle, N., Kippenberger, M., Schuster, G., & Crowley, J. N. (2010). The interaction of h2o2 with ice surfaces between 203 and 233 k. *Phys. Chem. Chem. Phys.*, *12*, 15544-15550. Retrieved from `http://dx.doi.org/10.1039/C0CP01656J` doi: 10.1039/C0CP01656J

Shimazaki, T., & Shimizu, M. (1979). The seasonal variation of ozone density in the martian atmosphere [Journal Article]. *Journal of Geophysical Research: Space Physics*, *84*(A4), 1269-1276. Retrieved from `https://agupubs.onlinelibrary.wiley.com/doi/abs/10.1029/JA084iA04p01269https://agupubs.onlinelibrary.wiley.com/doi/pdf/10.1029/JA084iA04p01269` doi: doi:10.1029/JA084iA04p01269

Smith, M. D. (2004). Interannual variability in tes atmospheric observations of mars during 1999–2003 [Journal Article]. *Icarus*, *167*(1), 148-165. Retrieved from `http://www.sciencedirect.com/science/article/pii/S0019103503002872https://ac.els-cdn.com/S0019103503002872/1-s2.0-S0019103503002872-main.pdf?_tid=134d7518-6e86-4870-946c-888afd3e1f3a&acdnat=1543573383_b8fcadfffcc7c60134deee13bb5416dd` doi: https://doi.org/10.1016/j.icarus.2003.09.010

Steele, L. J., Lewis, S. R., Patel, M. R., Montmessin, F., Forget, F., & Smith, M. D. (2014). The seasonal cycle of water vapour on mars from assimilation of thermal emission spectrometer data. *Icarus*, *237*, 97–115.

Vandaele, A. C., Lopez-Moreno, J.-J., Patel, M. R., Bellucci, G., Daerden, F., Ristic,

B., . . . Team, t. N. (2018). Nomad, an integrated suite of three spectrometers for the exomars trace gas mission: Technical description, science objectives and expected performance [Journal Article]. *Space Science Reviews*, *214*(5), 80. Retrieved from `https://doi.org/10.1007/s11214-018-0517-2https://link.springer.com/content/pdf/10.1007%2Fs11214-018-0517-2.pdf` doi: 10.1007/s11214-018-0517-2

Villanueva, G. L., G., L., Aoki, S., Stone, S. W., Brines, A., Thomas, I. R., . . . Vandaele, A. C. (2022). The deuterium isotopic ratio of water released from the martian caps as measured with tgo/nomad. *Geophysical Research Letters*. (Under Review)

Viúdez-Moreiras, D., Saiz-Lopez, A., Blaszczak-Boxe, C., Manfredi, J. R., & Yung, Y. (2019). Diurnal variation in mars equatorial odd oxygen species: Chemical production and loss mechanisms. *Icarus*, 113458.

Wolff, M. J., Clancy, R. T., Kahre, M. A., Haberle, R. M., Forget, F., Cantor, B. A., & Malin, M. C. (2019). Mapping water ice clouds on mars with mro/marci [Journal Article]. *Icarus*. Retrieved from `http://www.sciencedirect.com/science/article/pii/S0019103518307176` doi: https://doi.org/10.1016/j.icarus.2019.05.041